Vibrational Analysis of a Strongly Correlated System, Pentamethine Streptocyanine Dye, Based on Observed Infrared and Raman Spectra and Density Functional Calculations

Kazuhiko Furuya and Yoshio Inagaki

Ashigara Research Laboratories, Fuji Photo Film Co. Ltd., 210 Nakanuma, Minami Ashigara, Kanagawa 250-0193, Japan

Hajime Torii

Department of Chemistry, School of Science, The University of Tokyo, Bunkyo-ku, Tokyo 113-0033, Japan

Yukio Furukawa

Department of Chemistry, School of Science and Engineering, Waseda University, Shinjuku-ku, Tokyo 169-8555, Japan

Mitsuo Tasumi*

Department of Chemistry, Faculty of Science, Saitama University, Urawa, Saitama 338-8570, Japan

Received: May 22, 1998; In Final Form: August 12, 1998

Vibrational analysis is carried out for the organic (cationic) part of a pentamethine streptocyanine dye, $[(CH_3)_2N(CH)_5N(CH_3)_2]^+ClO_4^-$ (alias SC5), by measuring its infrared and Raman spectra in solution and in the polycrystalline state and by calculating the vibrational force field and the IR and Raman intensities by the ab initio molecular orbital and density functional methods. It is found that a reasonable set of structural parameters and vibrational force field can be obtained for the SC5 organic part at the BHandHLYP/6-31G* level. The observed features of the IR and Raman spectra, including relative intensities, are well reproduced by the calculations at this theoretical level. Two strong IR bands observed in the 1600−1200-cm^{-1} region arise from the delocalized b_1 modes along the bond-alternation coordinate of the conjugated chain. The strong IR intensities are explained by large charge fluxes induced by these modes due to the strong electron−vibration interaction. These modes also appear in the Raman spectrum in solution because of the interaction with the perchlorate ion existing at an asymmetric position near the conjugated chain. A delocalized a_1 mode of the conjugated chain gives rise to a strong Raman band. Examination of the IR and Raman intensities and the vibrational force constants clearly shows that the conjugated chain of the SC5 organic part is a strongly correlated system. A detailed analysis of the origin of the IR and Raman intensities shows that the potential energy distribution is not necessarily a good indicator of the origin of intensities.

1. Introduction

Cyanine dyes with conjugated methine chains act as spectral sensitizers in the silver halide photographic system.[1] By varying the chain lengths of these compounds, the photosensitive region of silver halides is extended to the visible or near-infrared region. Many studies have been performed on this spectral sensitization process,[2,3] from the viewpoints of both reaction dynamics and adsorption structures.

Cyanine dyes form J-aggregates when they are adsorbed on the surface of silver halide grains, with their electronic absorption spectra being narrowed and the spectral sensitivity sharpened. The spectral features of the J-bands have been interpreted with the exciton theory,[4,5] in which the dye molecules are approximated by building blocks adsorbed on the surface of silver halide grains. The relative position and orientation of the cyanine dyes on the surface have been estimated from the number of adsorbed dye molecules and the surface area. It has recently been reported[6,7] that polarized fluorescence microscopy is useful for studying the relative orientation of the cyanine dyes adsorbed on large silver halide grains. It is important to control the adsorption structures of cyanine dyes on silver halide grains for the purpose of improving the efficiency of spectral sensitization and hence the photographic sensitivity. However, the adsorption structures have not been clarified in sufficient detail at the molecular level.

As a basis for analyzing the adsorption structures of cyanine dyes at the molecular level by vibrational spectroscopy, it is important to examine the vibrational spectra of the dyes themselves. Among the previous studies on this subject,[8−12] a vibrational analysis of a cyanine dye has been carried out by Sano et al.[8] They have observed the infrared and Raman spectra of a pentamethine streptocyanine dye and its isotopically substituted species and have derived an empirical vibrational force field. By using this force field, reasonable agreement between the observed and calculated vibrational wavenumbers has been obtained in the high-wavenumber region but not in the region below 600 cm^{-1}. It may be said, therefore, that the vibrational force field as well as the other vibrational properties deserve further detailed analyses.

* Corresponding author. Fax: +81-48-858-3379. E-mail: tasumi@chem.saitama-u.ac.jp.

10.1021/jp9823502 CCC: $15.00
Published on Web 10/06/1998

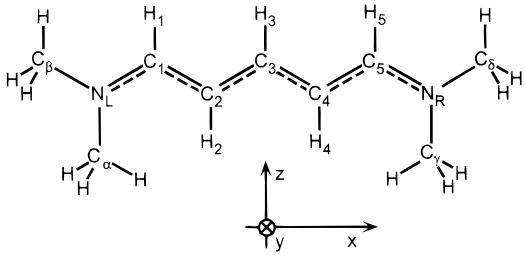

Figure 1. Coordinate axes and the numbering of atoms for the organic part of SC5.

In this context, it should be pointed out that the conjugated chains, in general, are correlated systems. For example, in the case of neutral polyene chains, it has been shown[13−15] that some off-diagonal (coupling) force constants are significantly large between the stretches of distant CC bonds in a chain. For charged polyene chains and related compounds, it has been shown[16] that strong IR intensities are induced by the skeletal CC stretches as a result of delocalized motions of the electrons (charge fluxes). It is, therefore, interesting to analyze the vibrational properties of cyanine dyes and examine how strongly their conjugated chains are correlated.

In the present paper, we study the IR and Raman spectra of the same pentamethine streptocyanine dye as treated by Sano et al.[8] [(5-dimethylaminopenta-2,4-dienylidene) ammonium perchlorate, $[(CH_3)_2N(CH)_5N(CH_3)_2]^+ClO_4^-$, alias SC5, see Figure 1] in more detail. The vibrational wavenumbers and the IR and Raman intensities obtained from ab initio molecular orbital (MO) and density functional (DF) calculations at various theoretical levels are compared with the experimental results. We discuss what theoretical level is appropriate to obtain a reliable vibrational force field, and analyze in detail the vibrational modes giving rise to strong IR and Raman bands.

2. Experimental and Computational Procedures

IR spectra were measured on Fourier transform IR spectrophotometers (Nicolet 5DX and Digilab FTS-40) at 4-cm^{-1} resolution. Spectra in the mid-IR region were measured in a dimethyl sulfoxide (DMSO) solution and in a KBr disk. Raman spectra were measured on a Fourier transform Raman spectrophotometer (Bruker RFS-100) at 2-cm^{-1} resolution, both in DMSO-d_6 solution and in the polycrystalline (powder) state.

Ab initio MO and DF calculations were performed by using the Gaussian 92/DFT and Gaussian 94 programs[17,18] on Kubota TITAN-3020 and Silicon Graphics Power Onyx workstations. The perchlorate ion was not included in the calculations. The Hartree−Fock (HF) and the second-order Møller−Plesset perturbation (MP2) methods were employed in combination with the 6-31G* basis set in the ab initio MO calculations. All the electrons were included in the treatment of electron correlation in the calculations at the MP2 level. DF calculations were performed by using the following three exchange-correlation functionals: BLYP (Becke 88 exchange[19] and Lee−Yang−Parr correlation[20,21]), B3LYP (Becke's three-parameter hybrid method[22] with the Lee−Yang−Parr correlation), and BHandHLYP (Becke's half-and-half hybrid method[23] with the Lee−Yang−Parr correlation). The 6-31G* basis set was employed in all DF calculations. Numerical integration of functionals was performed by using the "fine" integration grid in both the Gaussian 92/DFT and Gaussian 94 programs. The IR and Raman intensities were calculated at the BHandHLYP/6-31G* level from the dipole derivatives and polarizability derivatives computed from the potential energy gradients under a finite electric field by the mothod of Komornicki and McIver.[24]

TABLE 1: Structural Parameters of the Organic Part of SC5[a]

		calc[c]				
	obs[b]	HF	MP2	BLYP	B3LYP	BHandHLYP
$r(N_LC_1)$	1.312	1.308	1.324	1.343	1.328	1.314
$r(C_1C_2)$	1.382	1.387	1.393	1.403	1.394	1.385
$r(C_2C_3)$	1.388	1.388	1.391	1.405	1.395	1.386
$r(N_LC_\alpha)$	1.458	1.460	1.462	1.479	1.466	1.455
$r(N_LC_\beta)$	1.453	1.459	1.462	1.477	1.465	1.454
$\theta(N_LC_1C_2)$	126.6	127.3	126.3	126.7	126.7	126.8
$\theta(C_1C_2C_3)$	121.5	119.4	119.4	120.7	120.3	119.8
$\theta(C_2C_3C_4)$	124.5	126.1	125.7	125.6	125.7	126.0
$\theta(C_\alpha N_LC_1)$	123.1	121.2	120.9	121.3	121.2	121.1
$\theta(C_\beta N_LC_1)$	120.5	121.6	121.7	121.5	121.6	121.7
$\theta(C_\alpha N_LC_\beta)$	116.6	117.2	117.5	117.2	117.2	117.3

[a] In units of angstroms (bond lengths) and degrees (bond angles). [b] X-ray diffraction, ref 25. [c] The 6-31G* basis set is used.

Based on the vibrational force fields obtained from the ab initio MO and DF calculations, vibrational analyses were carried out with the programs written by one of the authors (H.T.) on M880 and S-3800 computers at the Computer Center of the University of Tokyo.

3. Results and Discussion

A. Structural Parameters. In the present calculations, it is assumed that the SC5 organic part (hereafter abbreviated as SC5OP) has C_{2v} symmetry. Under this symmetry, four conformations are possible with respect to the internal rotation of the methyl groups. Only one of them, which is depicted in Figure 1, is found to be at a potential energy minimum, and this conformation is used for the subsequent calculations. In this conformation, the α and γ methyl groups are rotated by ∼60° from the structure found in crystal.[25]

In Table 1, some structural parameters calculated at various theoretical levels are compared with those observed.[25] The bond lengths are generally overestimated at the MP2, BLYP, and B3LYP levels, whereas those calculated at the HF and BHandHLYP levels are in reasonable agreement with the experimental results. As for the bond angles, the agreement between the observed and calculated values is reasonable at all the theoretical levels.

The CC bond lengths $r(C_1C_2)$ and $r(C_2C_3)$ are close to each other, indicating that SC5OP has essentially no bond alternation in its molecular skeleton. This result is in contrast to the case of linear oligoenes with an even number of carbon atoms in the conjugated chain, in which the C═C bonds are substantially shorter than the C−C bonds.[14,26]

B. Observed Spectra. The observed IR and Raman spectra of SC5 in solution and in the polycrystalline state (KBr disk or powder) are shown in Figures 2a, 3a, and 4. Solvent bands are subtracted in the spectra observed in solution.

The wavenumbers of the IR bands observed in DMSO solution are in agreement with those observed in $CHCl_3$ solution[8] within 5 cm^{-1}, except that the 598-cm^{-1} band is observed for the first time in the present study. The IR bands observed in KBr disk are significantly broader than those in DMSO solution. A few IR bands are seen in KBr disk but not in DMSO solution, partly because of the overlap of residual solvent bands in the latter.

Contrary to the case of the IR bands, sharp Raman bands are observed both in solution and in the polycrystalline state. Measurement of the degrees of depolarization (not shown) indicates that all the Raman bands observed in solution are polarized. Two additional Raman bands are observed at 1574

TABLE 2: Observed and Calculated Vibrational Wavenumbers (in cm^{-1}) of the Organic Part of SC5[a]

			calc[c]				
		obs[b]	HF	MP2	BLYP	B3LYP	BHandHLYP
a_1	ν_8	1658	1657	1688	1650	1663	1673
	ν_9		1502	1496	1504	1497	1498
	ν_{10}	1495	1490	1486	1495	1485	1482
	ν_{11}	1446	1463	1447	1460	1453	1453
	ν_{12}	1416	1442	1430	1437	1431	1432
	ν_{13}	1416	1434	1420	1410	1416	1424
	ν_{14}		1372	1356	1363	1360	1363
	ν_{15}	1302	1296	1289	1291	1290	1294
	ν_{16}	1258[d]	1258	1265	1274	1268	1263
	ν_{17}	1196[d]	1193	1188	1179	1185	1193
	ν_{18}	1132	1125	1116	1116	1116	1120
	ν_{19}	1060[d]	1053	1051	1040	1047	1054
	ν_{20}	853	827	836	825	834	840
	ν_{21}	615[d]	599	598	604	602	600
	ν_{22}	475	452	452	457	455	453
	ν_{23}		320	321	322	320	320
	ν_{24}	253	228	230	232	230	229
	ν_{25}		65	63	65	64	63
b_1	ν_{32}	1603	1610	1610	1586	1600	1614
	ν_{33}	1570	1529	1631	1608	1598	1574
	ν_{34}		1495	1489	1497	1488	1486
	ν_{35}		1481	1476	1485	1476	1473
	ν_{36}	1416	1444	1427	1441	1435	1434
	ν_{37}		1438	1424	1435	1428	1427
	ν_{38}	1397	1404	1397	1393	1396	1402
	ν_{39}		1307	1300	1301	1298	1301
	ν_{40}		1249	1249	1251	1250	1253
	ν_{41}	1206	1199	1230	1244	1230	1207
	ν_{42}		1146	1188	1190	1191	1193
	ν_{43}		1093	1101	1100	1101	1103
	ν_{44}		1051	1050	1040	1046	1053
	ν_{45}	856	835	843	834	842	847
	ν_{46}	598	581	582	585	586	585
	ν_{47}		460	456	460	459	458
	ν_{48}		379	378	383	380	379
	ν_{49}		172	172	171	170	171
b_2	ν_{50}		1477	1469	1480	1470	1468
	ν_{51}		1463	1456	1467	1457	1455
	ν_{52}		1149	1130	1137	1135	1139
	ν_{53}		1108	1089	1096	1093	1096
	ν_{54}	1016[d]	1053	982	1007	1010	1024
	ν_{55}		968	886	894	907	930
	ν_{56}	859[d]	857	807	853	854	856
	ν_{57}	472[d]	471	453	455	461	467
	ν_{58}		266	261	265	265	266
	ν_{59}		230	231	229	230	232
	ν_{60}		151	158	151	157	159
	ν_{61}		82	56	57	67	77
	ν_{62}		49	47	50	51	50

[a] The CH stretching modes and the a_2 modes are not shown. [b] In DMSO or DMSO-d_6 unless otherwise stated. Raman for the a_1 modes and IR for the b_1 and b_2 modes. [c] The 6-31G* basis set is used. The calculated wavenumbers are uniformly scaled by using the scale factor of 0.900 for HF, 0.949 for MP2, 1.000 for BLYP, 0.968 for B3LYP, and 0.933 for BHandHLYP. [d] In a KBr disk.

and 1207 cm^{-1} in solution which are not observed in the polycrystalline state. Comparison between the observed and calculated vibrational wavenumbers (shown below) indicates that these two Raman bands arise from the same normal modes that give rise to the strong IR bands observed at 1570 and 1206 cm^{-1}. It is known that single crystals of SC5 take two forms: the yellow form and the orange form.[8] Raman bands are observed at 1582/1562 and 1201 cm^{-1} for the orange form, in which the perchlorate ion resides on one end of the conjugated chain of SC5OP. These bands are not observed for the yellow form (the crystal used in the present study), in which the perchlorate ions are located at symmetric positions. The experimental result that these bands are observed in solution indicates that the perchlorate ions are not always located at symmetric positions near the conjugated chains. The mechanism giving rise to strong Raman intensities for these bands is discussed later.

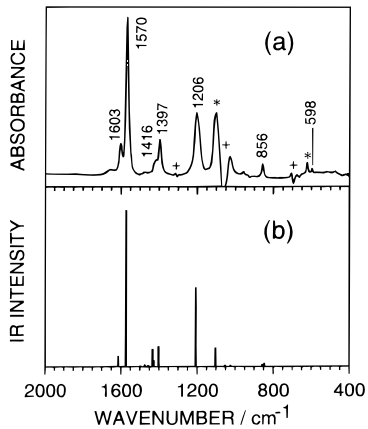

Figure 2. IR spectra of SC5 (a) observed in DMSO solution and (b) calculated at the BHandHLYP/6-31G* level. The solvent bands remaining after subtraction are marked with "+". The bands originating from the perchlorate ion are marked with "∗".

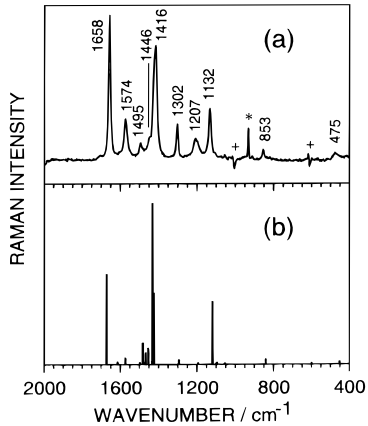

Figure 3. Raman spectra of SC5 (a) observed in DMSO-d_6 solution and (b) calculated at the BHandHLYP/6-31G* level. See footnote to Figure 2.

C. Comparison of the Results Obtained at Various Theoretical Levels. The vibrational wavenumbers calculated at various theoretical levels with the 6-31G* basis set are shown in Table 2. The calculated wavenumbers are uniformly scaled by a single scale factor at each theoretical level. The observed wavenumbers taken from Figures 2−4 are also shown for comparison. As shown in section 3B, the vibrational wavenumbers observed in solution are mostly in agreement with those in the polycrystalline state, except for the Raman bands observed at 1574 and 1207 cm^{-1} in solution (discussed below). This result suggests that the solvent effect on the vibrational wavenumbers of this compound is small and justifies the comparison of the observed wavenumbers with those calculated for the isolated ion.

Although the agreement between the observed and calculated wavenumbers is generally reasonable, noticeable differences are seen for a few vibrational modes. At the HF level, the largest difference occurs for ν_{33}. The wavenumber of this mode calculated at the HF level is 1529 cm^{-1}, which is lower by 41 cm^{-1} than the observed wavenumber (1570 cm^{-1}). In this mode, the adjacent CC bonds stretch and contract alternately. It therefore represents the vibration along the bond-alternation coordinate, or the so-called "effective conjugation coordinate".[27,28]

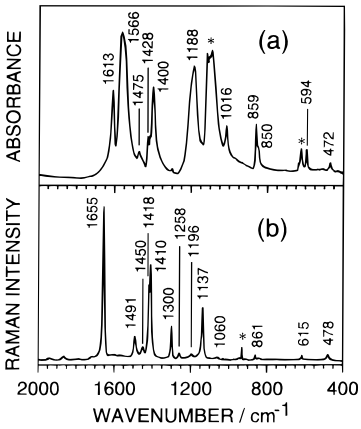

Figure 4. IR and Raman spectra of SC5 observed in the polycrystalline state: (a) IR and (b) Raman. See footnote to Figure 2.

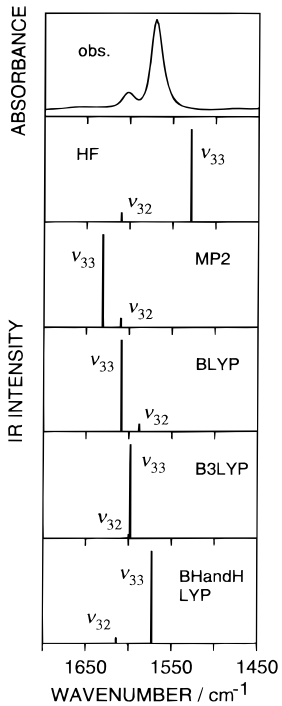

Figure 5. Observed and calculated IR spectra of SC5 in the 1700−1450-cm^{-1} region.

It is known that the effect of electron correlation is large on the wavenumber of this kind of vibrational mode of conjugated π-electron systems, such as linear polyenes,[13−15,29−32] benzene,[33−36] and other aromatic systems.[36−38] The IR spectra of SC5 in the 1700−1450-cm^{-1} region calculated at various theoretical levels are compared with the observed spectrum in Figure 5. The IR bands arising from ν_{32} and ν_{33} are seen in this wavenumber region, with the calculated IR intensity of ν_{33} being higher than the other at all the theoretical levels employed. At the HF level, the calculated wavenumber separation between the two modes ($\nu_{32} - \nu_{33} = 81$ cm^{-1}) is too large as compared with the observed value (33 cm^{-1}). By contrast, ν_{33} is calculated to be higher in wavenumber than ν_{32} at the MP2 and BLYP levels (with wavenumber separations of −21 and −22 cm^{-1}, respectively), contrary to the experimental results. At the B3LYP level, the calculated wavenumbers of the two modes are too close. Therefore, the vibrational force field of SC5OP is not calculated with sufficient accuracy at these four levels. As shown in Figure 5, the feature of the IR spectrum in the 1700−1450-cm^{-1} region is well reproduced only at the BHandHLYP level among the five theoretical levels used in the present study.

TABLE 3: Definition of the In-Plane Molecular Symmetry Coordinates of the Organic Part of SC5

symmetry	coordinate	abbreviation	definition[a]
a_1	S_1	NC_1 str	$[\sigma(N_LC_1) + \sigma(N_RC_5)]/\sqrt{2}$
	S_2	C_1C_2 str	$[\sigma(C_1C_2) + \sigma(C_4C_5)]/\sqrt{2}$
	S_3	C_2C_3 str	$[\sigma(C_2C_3) + \sigma(C_3C_4)]/\sqrt{2}$
	S_4	NC_α str	$[\sigma(N_LC_\alpha) + \sigma(N_RC_\gamma)]/\sqrt{2}$
	S_5	NC_β str	$[\sigma(N_LC_\beta) + \sigma(N_RC_\delta)]/\sqrt{2}$
	S_6	C_1H_1 str	$[\sigma(C_1H_1) + \sigma(C_5H_5)]/\sqrt{2}$
	S_7	C_2H_2 str	$[\sigma(C_2H_2) + \sigma(C_4H_4)]/\sqrt{2}$
	S_8	C_3H_3 str	$\sigma(C_3H_3)$
	S_9	Me_α sym str	$[\sigma_s(Me_\alpha) + \sigma_s(Me_\gamma)]/\sqrt{2}$
	S_{10}	Me_α ip asym str	$[\sigma_{a,ip}(Me_\alpha) + \sigma_{a,ip}(Me_\gamma)]/\sqrt{2}$
	S_{11}	Me_β sym str	$[\sigma_s(Me_\beta) + \sigma_s(Me_\delta)]/\sqrt{2}$
	S_{12}	Me_β ip asym str	$[\sigma_{a,ip}(Me_\beta) + \sigma_{a,ip}(Me_\delta)]/\sqrt{2}$
	S_{13}	NC_1C_2 bend	$[\delta(N_LC_1C_2) + \delta(N_RC_5C_4)]/\sqrt{2}$
	S_{14}	$C_1C_2C_3$ bend	$[\delta(C_1C_2C_3) + \delta(C_3C_4C_5)]/\sqrt{2}$
	S_{15}	$C_2C_3C_4$ bend	$\delta(C_2C_3C_4)$
	S_{16}	C_1H_1 bend	$[\delta(C_1H_1) + \delta(C_5H_5)]/\sqrt{2}$
	S_{17}	C_2H_2 bend	$[\delta(C_2H_2) + \delta(C_4H_4)]/\sqrt{2}$
	S_{18}	$C_\alpha NC_\beta$ bend	$[\delta(C_\alpha N_LC_\beta) + \delta(C_\gamma N_RC_\delta)]/\sqrt{2}$
	S_{19}	$C_\alpha NC_\beta$ rock	$[\gamma(C_\alpha N_LC_\beta) + \gamma(C_\gamma N_RC_\delta)]/\sqrt{2}$
	S_{20}	Me_α sym bend	$[\delta_s(Me_\alpha) + \delta_s(Me_\gamma)]/\sqrt{2}$
	S_{21}	Me_α ip asym bend	$[\delta_{a,ip}(Me_\alpha) + \delta_{a,ip}(Me_\gamma)]/\sqrt{2}$
	S_{22}	Me_α ip rock	$[\gamma_{ip}(Me_\alpha) + \gamma_{ip}(Me_\gamma)]/\sqrt{2}$
	S_{23}	Me_β sym bend	$[\delta_s(Me_\beta) + \delta_s(Me_\delta)]/\sqrt{2}$
	S_{24}	Me_β ip asym bend	$[\delta_{a,ip}(Me_\beta) + \delta_{a,ip}(Me_\delta)]/\sqrt{2}$
	S_{25}	Me_β ip rock	$[\gamma_{ip}(Me_\beta) + \gamma_{ip}(Me_\delta)]/\sqrt{2}$
b_1	S_{26}	NC_1 str	$[\sigma(N_LC_1) - \sigma(N_RC_5)]/\sqrt{2}$
	S_{27}	C_1C_2 str	$[\sigma(C_1C_2) - \sigma(C_4C_5)]/\sqrt{2}$
	S_{28}	C_2C_3 str	$[\sigma(C_2C_3) - \sigma(C_3C_4)]/\sqrt{2}$
	S_{29}	NC_α str	$[\sigma(N_LC_\alpha) - \sigma(N_RC_\gamma)]/\sqrt{2}$
	S_{30}	NC_β str	$[\sigma(N_LC_\beta) - \sigma(N_RC_\delta)]/\sqrt{2}$
	S_{31}	C_1H_1 str	$[\sigma(C_1H_1) - \sigma(C_5H_5)]/\sqrt{2}$
	S_{32}	C_2H_2 str	$[\sigma(C_2H_2) - \sigma(C_4H_4)]/\sqrt{2}$
	S_{33}	Me_α sym str	$[\sigma_s(Me_\alpha) - \sigma_s(Me_\gamma)]/\sqrt{2}$
	S_{34}	Me_α ip asym str	$[\sigma_{a,ip}(Me_\alpha) - \sigma_{a,ip}(Me_\gamma)]/\sqrt{2}$
	S_{35}	Me_β sym str	$[\sigma_s(Me_\beta) - \sigma_s(Me_\delta)]/\sqrt{2}$
	S_{36}	Me_β ip asym str	$[\sigma_{a,ip}(Me_\beta) - \sigma_{a,ip}(Me_\delta)]/\sqrt{2}$
	S_{37}	NC_1C_2 bend	$[\delta(N_LC_1C_2) - \delta(N_RC_5C_4)]/\sqrt{2}$
	S_{38}	$C_1C_2C_3$ bend	$[\delta(C_1C_2C_3) - \delta(C_3C_4C_5)]/\sqrt{2}$
	S_{39}	C_1H_1 bend	$[\delta(C_1H_1) - \delta(C_5H_5)]/\sqrt{2}$
	S_{40}	C_2H_2 bend	$[\delta(C_2H_2) - \delta(C_4H_4)]/\sqrt{2}$
	S_{41}	C_3H_3 bend	$\delta(C_3H_3)$
	S_{42}	$C_\alpha NC_\beta$ bend	$[\delta(C_\alpha N_LC_\beta) - \delta(C_\gamma N_RC_\delta)]/\sqrt{2}$
	S_{43}	$C_\alpha NC_\beta$ rock	$[\gamma(C_\alpha N_LC_\beta) - \gamma(C_\gamma N_RC_\delta)]/\sqrt{2}$
	S_{44}	Me_α sym bend	$[\delta_s(Me_\alpha) - \delta_s(Me_\gamma)]/\sqrt{2}$
	S_{45}	Me_α ip asym bend	$[\delta_{a,ip}(Me_\alpha) - \delta_{a,ip}(Me_\gamma)]/\sqrt{2}$
	S_{46}	Me_α ip rock	$[\gamma_{ip}(Me_\alpha) - \gamma_{ip}(Me_\gamma)]/\sqrt{2}$
	S_{47}	Me_β sym bend	$[\delta_s(Me_\beta) - \delta_s(Me_\delta)]/\sqrt{2}$
	S_{48}	Me_β ip asym bend	$[\delta_{a,ip}(Me_\beta) - \delta_{a,ip}(Me_\delta)]/\sqrt{2}$
	S_{49}	Me_β ip rock	$[\gamma_{ip}(Me_\beta) - \gamma_{ip}(Me_\delta)]/\sqrt{2}$

[a] Defined by using local coordinates represented by symbols. σ, stretching; δ, bending; γ, rocking; s, symmetric; as, antisymmetric; ip, in-plane.

It is clear from Table 2 that the vibrational wavenumbers calculated at the BHandHLYP level are in agreement with the observed wavenumbers also for the other vibrational modes. In Figures 2 and 3 are shown the IR and Raman spectra in the 2000−400-cm^{-1} region calculated at the BHandHLYP level in

TABLE 4: Vibrational Wavenumbers, IR and Raman Intensities, and Assignments of the In-Plane Normal Modes of the Organic Part of SC5

		obs[a]		calc[b]					
		wavenumber/ cm^{-1}	intensity	wavenumber[c]/ cm^{-1}	IR intensity/km mol^{-1}	Raman activity/$Å^4$ amu^{-1}	assignments (PED)		
a_1	ν_8	1658	s	1673	0.6	199.6	NC_1 str(48)	C_1C_2 str(33)	C_1H_1 bend(20)
	ν_9			1498	26.9	5.1	Me_β ip asym bend(40)	Me_β ip rock(12)	Me_α ip asym bend(12)
	ν_{10}	1495	w	1482	2.4	47.7	Me_α ip asym bend(59)	Me_β ip asym bend(29)	Me_α ip rock(9)
	ν_{11}	1446	w	1453	0.6	29.8	Me_β sym bend(37)	Me_α sym bend(30)	Me_β ip asym bend(10)
	ν_{12}	1416	s	1432	0.6	357.2	Me_β sym bend(65)	NC_1 str(10)	Me_β ip asym bend(8)
	ν_{13}	1416	s	1424	1.5	158.0	Me_α sym bend(69)	NC_1 str(12)	NC_α str(9)
	ν_{14}			1363	9.3	0.1	C_1H_1 bend(37)	C_2H_2 bend(27)	C_2C_3 str(9)
	ν_{15}	1302	m	1294	13.3	11.3	C_1H_1 bend(22)	C_1C_2 str(20)	C_2C_3 str(15)
	ν_{16}	1258[d]	w	1263	0.2	0.2	C_2H_2 bend(44)	C_2C_3 str(22)	C_1C_2 str(13)
	ν_{17}	1196[d]	w	1193	11.6	2.4	Me_α ip rock(28)	C_2C_3 str(22)	NC_β str(20)
	ν_{18}	1132	m	1120	3.9	138.8	Me_β ip rock(53)	NC_1 str(12)	Me_α ip rock(8)
	ν_{19}	1060[d]	w	1054	35.0	4.0	Me_α ip rock(37)	NC_α str(21)	Me_β ip rock(21)
	ν_{20}	853	w	840	1.5	12.6	NC_α str(47)	NC_β str(32)	
	ν_{21}	615[d]	w	600	2.2	3.9	NC_1C_2 bend(34)	$C_\alpha NC_\beta$ rock(30)	$C_2C_3C_4$ bend(27)
	ν_{22}	475	w	453	0.6	6.6	$C_\alpha NC_\beta$ bend(68)		
	ν_{23}			320	1.6	1.0	$C_\alpha NC_\beta$ rock(46)	$C_2C_3C_4$ bend(24)	NC_1C_2 bend(9)
	ν_{24}	253	s	229	0.1	55.2	$C_\alpha NC_\beta$ bend(19)	$C_1C_2C_3$ bend(17)	NC_1C_2 bend(14)
	ν_{25}			63	0.4	1.0	$C_1C_2C_3$ bend(53)	$C_2C_3C_4$ bend(36)	NC_1C_2 bend(21)
b_1	ν_{32}	1603	m	1614	264.8	6.5	NC_1 str(43)	C_2C_3 str(24)	C_3H_3 bend(10)
	ν_{33}	1570	vs	1574	3923.3	15.6	C_2C_3 str(34)	C_1C_2 str(24)	C_2H_2 bend(20)
	ν_{34}			1486	9.6	2.2	Me_β ip asym bend(78)	Me_β ip rock(12)	
	ν_{35}			1473	53.4	4.3	Me_α ip asym bend(83)	Me_α ip rock(10)	
	ν_{36}	1416	w	1434	441.4	9.5	Me_α sym bend(59)	Me_β sym bend(27)	C_1H_1 bend(15)
	ν_{37}			1427	161.4	61.0	Me_β sym bend(72)	Me_α sym bend(35)	
	ν_{38}	1397	m	1402	503.5	0.6	C_1H_1 bend(24)	NC_1 str(18)	NC_α str(16)
	ν_{39}			1301	0.1	2.4	C_3H_3 bend(42)	NC_1C_2 bend(11)	C_2C_3 str(9)
	ν_{40}			1253	4.8	1.1	C_2H_2 bend(18)	NC_β str(17)	C_1C_2 str(17)
	ν_{41}	1206	s	1207	1967.5	0.1	C_1C_2 str(41)	C_2C_3 str(17)	C_2H_2 bend(11)
	ν_{42}			1193	5.0	4.1	C_2H_2 bend(38)	C_1H_1 bend(18)	C_3H_3 bend(14)
	ν_{43}			1103	472.4	2.5	Me_β ip rock(45)	NC_1 str(18)	Me_α ip rock(10)
	ν_{44}			1053	39.4	1.6	Me_α ip rock(37)	Me_β ip rock(23)	NC_α str(20)
	ν_{45}	856	w	847	80.2	0.2	NC_α str(49)	NC_β str(24)	NC_1C_2 bend(9)
	ν_{46}	598	vw	585	7.5	1.7	NC_1C_2 bend(28)	NC_β str(17)	$C_\alpha NC_\beta$ rock(11)
	ν_{47}			458	1.9	0.2	$C_\alpha NC_\beta$ rock(46)	$C_1C_2C_3$ bend(35)	$C_\alpha NC_\beta$ bend(14)
	ν_{48}			379	0.4	0.2	$C_\alpha NC_\beta$ bend(73)	$C_1C_2C_3$ bend(14)	
	ν_{49}			171	0.1	2.0	NC_1C_2 bend(46)	$C_1C_2C_3$ bend(27)	$C_\alpha NC_\beta$ rock(21)

[a] Raman in DMSO-d_6 for the a_1 modes and IR in DMSO for the b_1 modes. [b] At the BHandHLYP/6-31G* level. [c] Uniformly scaled by 0.933. [d] In a KBr disk.

comparison with those observed in solution. Except for the Raman bands observed at 1574 and 1207 cm^{-1} (discussed below), the observed features of both spectra are mostly reproduced by the calculations. It is therefore concluded that the calculations at the BHandHLYP level provide reasonable estimates for the vibrational force field and the dipole and polarizability derivatives of SC5OP. In the following section, we analyze the vibrational modes of SC5OP on the basis of the calculations at this theoretical level.

D. IR and Raman Intensities, Band Assignments, and Force Constants. The in-plane molecular symmetry coordinates of SC5OP are defined as shown in Table 3, with the numbering of atoms shown in Figure 1. Various properties of normal modes, including their IR and Raman intensities, and vibrational force constants are examined by using this coordinate system.

The calculated vibrational wavenumbers and the IR and Raman intensities of the in-plane normal modes of SC5OP, together with their assignments based on potential energy distribution (PED), are shown in Table 4 in comparison with the observed wavenumbers and intensities taken from Figures 2−4. The vibrational patterns of the modes with strong IR and Raman intensities are shown in Figure 6.

The strong IR bands observed at 1570 and 1206 cm^{-1} (ν_{33} and ν_{41}) are assigned to delocalized vibrations of the conjugated chain mixed with the CH bends. As shown in Figure 6, adjacent CC bonds stretch and contract alternately in these modes. Such a vibration induces a large charge flux in the molecular skeleton of a charged polyene chain,[16,27,28,39,40] because this vibration corresponds to the transition between two resonance structures having an electric charge on the opposite ends of the chain. In other words, the electronic wave function changes significantly by this vibration because of the strong electron−vibration interaction.

As is well known, the IR intensity of the mth normal mode, Q_m, is proportional to $|\partial\boldsymbol{\mu}/\partial Q_m|^2$, where $\boldsymbol{\mu}$ is the dipole moment of the molecule. In the present case, if the x axis is chosen

TABLE 5: Dipole Derivatives ($\partial\mu_x/\partial S_j$, in D $Å^{-1}$) of the b_1 Symmetry Coordinates of the Organic Part of SC5[a]

coordinate	$\partial\mu_x/\partial S_j$	coordinate	$\partial\mu_x/\partial S_j$
S_{26}	16.817	S_{38}	0.450
S_{27}	−14.446	S_{39}	−0.376
S_{28}	15.025	S_{40}	−0.095
S_{29}	−3.453	S_{41}	0.144
S_{30}	−4.022	S_{42}	0.755
S_{31}	−0.026	S_{43}	−0.975
S_{32}	0.119	S_{44}	0.332
S_{33}	0.819	S_{45}	−0.664
S_{34}	0.055	S_{46}	−0.151
S_{35}	1.016	S_{47}	0.742
S_{36}	−0.596	S_{48}	0.413
S_{37}	0.453	S_{49}	−0.927

[a] Calculated at the BHandHLYP/6-31G* level.

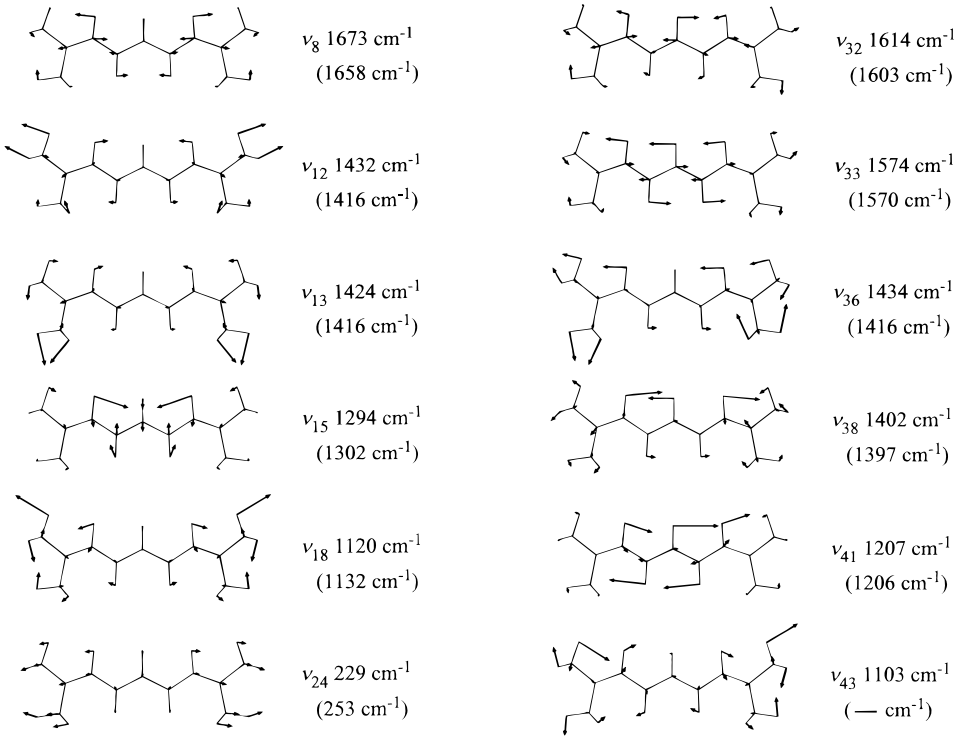

Figure 6. Vibrational patterns of the modes inducing strong IR and Raman intensities. The mode numbers and the calculated (observed) wavenumbers are indicated.

along the long axis of SC5OP as shown in Figure 1, a normal mode of b_1 symmetry may have a nonzero value of the dipole derivative $\partial\mu_x/\partial Q_m$, which can be expressed as

$$\frac{\partial \mu_x}{\partial Q_m} = \sum_j \frac{\partial \mu_x}{\partial S_j}\frac{\partial S_j}{\partial Q_m}$$

The calculated dipole derivatives $\partial\mu_x/\partial S_j$ for the b_1 symmetry coordinates are shown in Table 5, where the values are large for S_{26}, S_{27}, and S_{28}, which represent the CC and NC stretches of the conjugated chain. The contributions of the vibration along each symmetry coordinate to the IR intensity of a normal mode are examined by calculating the values of $\partial\mu_x/\partial S_j \times \partial S_j/\partial Q_m$, which are shown in Table 6. The CC and NC stretches (S_{26}, S_{27}, and S_{28}) contribute to the IR intensities of both ν_{33} and ν_{41} without mutual cancellation. This is the reason these two normal modes have large IR intensities.

As mentioned in section 3B, these two modes appear strongly also in the Raman spectrum in solution. When the perchlorate ion resides at an asymmetric position near the conjugated chain, the electric charge of the molecule moves along the chain by a slight deformation along the bond-alternation coordinate to reduce the potential energy arising from the Coulomb interaction. Because of the strong electron−vibration interaction, the electronic wave function changes substantially by this deformation. As a result, the *xx* component of the polarizability derivative for the bond-alternation coordinate increases significantly. The strong Raman bands at 1574 and 1207 cm^{-1} observed in solution are considered to arise by this mechanism. The detailed formulation based on a two-state model Hamiltonian will be described elsewhere.[41]

In Table 6, the values of $\partial\mu_x/\partial S_j \times \partial S_j/\partial Q_m$ are also shown for the other modes giving rise to the IR bands observed above 1000 cm^{-1} in solution, as well as ν_{43}, which is hidden under a perchlorate band. The mode ν_{32}, which is observed at 1603 cm^{-1}, consists mainly of the CC and NC stretches (S_{26} and S_{28})

TABLE 6: $\partial\mu_x/\partial S_j \times \partial S_j/\partial Q_m$ (in D Å^{-1} amu$^{-1/2}$) and the Potential Energy Distribution (in Percent) of the Strongly IR-Active b_1 Modes of the Organic Part of SC5

mode	coordinate	$\partial\mu_x/\partial S_j \times \partial S_j/\partial Q_m$	PED
ν_{32}	S_{26}	4.747	42.6
	S_{27}	0.994	2.0
	S_{28}	−3.711	24.0
	S_{30}	0.392	3.0
	total	2.503	
ν_{33}	S_{26}	2.553	13.0
	S_{27}	3.327	23.7
	S_{28}	4.309	34.0
	S_{39}	−0.246	17.4
	S_{40}	0.071	19.7
	S_{41}	−0.087	13.8
	total	9.636	
ν_{36}	S_{26}	0.608	0.9
	S_{27}	1.240	4.0
	S_{30}	0.383	3.6
	S_{39}	−0.207	14.8
	S_{44}	0.354	58.6
	S_{47}	0.530	26.5
	total	3.232	
ν_{38}	S_{26}	2.685	18.1
	S_{27}	−0.598	1.0
	S_{28}	0.763	1.3
	S_{29}	0.671	15.7
	S_{39}	0.257	23.8
	S_{48}	−0.206	12.0
	total	3.452	
ν_{41}	S_{26}	0.745	1.9
	S_{27}	3.344	40.7
	S_{28}	2.321	16.8
	S_{40}	−0.041	11.3
	S_{41}	0.059	10.9
	total	6.824	
ν_{43}	S_{26}	2.080	17.5
	S_{27}	−0.675	2.0
	S_{28}	0.981	3.6
	S_{30}	0.449	8.4
	S_{49}	0.592	45.1
	total	3.343	

TABLE 7: Polarizability Derivatives ($\partial\alpha_{xx}/\partial S_j$, $\partial\alpha_{yy}/\partial S_j$, and $\partial\alpha_{zz}/\partial S_j$, in Å^2) of the a_1 Symmetry Coordinates of the Organic Part of SC5[a]

coordinate	$\partial\alpha_{xx}/\partial S_j$	$\partial\alpha_{yy}/\partial S_j$	$\partial\alpha_{zz}/\partial S_j$
S_1	29.830	0.283	1.165
S_2	14.440	0.175	0.975
S_3	14.246	0.292	0.856
S_4	−0.924	−0.013	2.797
S_5	−2.380	0.009	1.544
S_6	−0.636	0.158	2.500
S_7	1.727	0.098	2.337
S_8	−0.919	0.101	1.699
S_9	3.887	2.222	1.855
S_{10}	3.286	−1.491	−0.671
S_{11}	6.833	2.278	1.818
S_{12}	−4.617	−1.533	2.144
S_{13}	2.436	−0.056	−0.249
S_{14}	8.050	−0.044	0.159
S_{15}	−0.192	−0.044	−0.211
S_{16}	−0.239	0.005	0.046
S_{17}	0.313	0.016	−0.055
S_{18}	−3.866	0.005	0.123
S_{19}	1.668	0.087	0.302
S_{20}	0.000	−0.178	0.764
S_{21}	0.223	0.408	−0.150
S_{22}	0.604	0.118	−0.424
S_{23}	1.448	−0.173	0.210
S_{24}	−2.033	0.428	0.218
S_{25}	−1.231	0.091	0.498

[a] Calculated at the BHandHLYP/6-31G* level.

in terms of PED. In this respect, this mode is similar to ν_{33} and ν_{41}. However, S_{26} and S_{28} cancel each other in theircontributions to the IR intensity of ν_{32}. This cancellation results from the opposite phases of the vibrations along S_{26} and S_{28} in this normal mode, as shown in Figure 6. The IR intensity of this mode is, therefore, weaker than those of ν_{33} and ν_{41}. The two IR bands observed at 1416 and 1397 cm^{-1} (ν_{36} and ν_{38}) arise mainly from the methyl symmetric bend (S_{44}) and the CH bend (S_{39}), respectively, in terms of PED. However, the contributions of these coordinates to the IR intensities of the two modes are rather small. As shown in Table 6, the IR intensities of these modes mostly derive from the CC and NC stretches in terms of $\partial\mu_x/\partial S_j \times \partial S_j/\partial Q_m$. It should be especially noted that the largest contribution to the IR intensity of ν_{36} comes from S_{27}, for which the PED is only 4%. In the case of ν_{43} (calc 1103 cm^{-1}), the PED is largest for S_{49} (methyl rock), while S_{26} has the largest contribution to the IR intensity. This result indicates that PED is not necessarily a good indicator of the origin of the IR intensity. The IR intensities are primarily determined by the contributions of the coordinates having large values of $\partial\mu_x/\partial S_j$, when the values of $\partial\mu_x/\partial S_j$ are significantly different from coordinate to coordinate.

The strong Raman band observed at 1658 cm^{-1} (ν_8) is assigned to a delocalized vibration of the conjugated chain mixed with the CH bends. As shown in Figure 6, adjacent CC and NC bonds stretch and contract alternately. The vibrational pattern of this mode is, therefore, similar to those of ν_{33} and ν_{41}, except that ν_8 belongs to the a_1 symmetry species. The calculated polarizability derivatives of the a_1 symmetry coordinates are shown in Table 7. The values of the *xx* component of the polarizability derivative ($\partial\alpha_{xx}/\partial S_j$) are large for S_1, S_2, and S_3, which represent the CC and NC stretches of the conjugated chain. Since the conjugated chain extends along the *x* axis, the large values of $\partial\alpha_{xx}/\partial S_j$ for the CC and NC stretches arise from the mobility of electrons along the chain. The values of $\partial\alpha_{xx}/\partial S_j \times \partial S_j/\partial Q_m$ are shown in Table 8. Although the contributions of S_1 and S_2 to the Raman intensity

TABLE 8: $\partial\alpha_{xx}/\partial S_j \times \partial S_j/\partial Q_m$ (in Å^2 amu$^{-1/2}$) and the Potential Energy Distribution (in Percent) of the Strongly Raman-Active a_1 Modes of the Organic Part of SC5

mode	coordinate	$\partial\alpha_{xx}/\partial S_j \times \partial S_j/\partial Q_m$	PED
ν_8	S_1	9.093	48.2
	S_2	−4.057	33.0
	S_3	1.304	3.7
	S_{14}	−0.544	0.2
	S_{16}	−0.178	20.0
	S_{18}	−0.717	1.9
	total	4.065	
ν_{12}	S_1	3.618	10.4
	S_2	0.462	0.6
	S_3	−0.667	1.3
	S_{18}	−0.642	2.0
	S_{23}	1.611	64.8
	S_{24}	0.822	7.6
	total	5.493	
ν_{13}	S_1	3.812	11.6
	S_2	0.862	2.0
	S_3	−0.762	1.8
	S_{14}	−0.384	0.1
	S_{18}	−0.686	2.3
	S_{20}	0.000	68.9
	S_{23}	−0.374	3.5
	S_{24}	0.840	8.0
	total	3.551	
ν_{15}	S_1	0.404	0.2
	S_2	2.411	19.6
	S_3	2.026	15.1
	S_{13}	−0.896	13.2
	S_{14}	−3.500	14.4
	S_{16}	−0.143	21.6
	S_{19}	0.418	6.5
	total	0.723	
ν_{18}	S_1	3.099	12.5
	S_2	0.689	2.1
	S_{14}	−1.265	2.5
	S_{18}	0.388	1.2
	S_{24}	−0.446	3.7
	S_{25}	0.862	52.8
	total	3.414	
ν_{24}	S_1	0.399	4.9
	S_3	0.325	12.3
	S_{13}	0.164	14.1
	S_{14}	0.666	16.6
	S_{18}	0.315	19.1
	total	2.129	

partially cancel each other, the very large magnitude of the value for S_1 results in the strong Raman intensity of ν_8.

The strong Raman band observed at 1416 cm^{-1} is considered to be an overlapped band of ν_{12} and ν_{13}, both of which mainly consist of the methyl symmetric bend (S_{20} and S_{23}) in terms of PED. However, as shown in Table 8, the Raman intensities of these modes primarily derive from the vibrations along S_1, for which the PED is only 10−12%. The Raman band with a medium intensity observed at 1132 cm^{-1} (ν_{18}) consists mainly of the methyl rock (S_{25}) in terms of PED. In this case also, a great part of the Raman intensity comes from the vibration along S_1 (with PED of 12%). Like the cases of the IR intensities of some modes discussed above, PED is not necessarily a good indicator of the origin of the Raman intensity.

The Raman band with a medium intensity observed at 1302 cm^{-1} corresponds to ν_{15}, which consists of the C_1H_1 bend (S_{16}) mixed with the CC stretches (S_2 and S_3) and the CCC and NCC bends (S_{13} and S_{14}). As shown in Table 8, this mode does not induce a strong Raman intensity because of the mutual cancellation of the contributions from S_2, S_3, and S_{14}. It has been pointed out[42,43] that the ν_{15} Raman band can be used as a marker

TABLE 9: Skeletal Stretching Force Constants of the Organic Part of SC5[a]

coordinate	force constants/mdyn Å^{-1}
Diagonal Terms	
$\sigma(N_LC_1)$	8.376
$\sigma(C_1C_2)$	6.712
$\sigma(C_2C_3)$	6.692
$\sigma(N_LC_\alpha)$	4.821
$\sigma(N_LC_\beta)$	4.860
Off-Diagonal Terms	
$\sigma(N_LC_1)/\sigma(C_1C_2)$	0.852
$\sigma(N_LC_1)/\sigma(C_2C_3)$	−0.317
$\sigma(N_LC_1)/\sigma(C_3C_4)$	0.242
$\sigma(N_LC_1)/\sigma(C_4C_5)$	−0.175
$\sigma(N_LC_1)/\sigma(N_RC_5)$	0.169
$\sigma(C_1C_2)/\sigma(C_2C_3)$	0.595
$\sigma(C_1C_2)/\sigma(C_3C_4)$	−0.272
$\sigma(C_1C_2)/\sigma(C_4C_5)$	0.181
$\sigma(C_2C_3)/\sigma(C_3C_4)$	0.658

[a] Calculated at the BHandHLYP/6-31G* level. Uniformly scaled by $(0.933)^2$.

for discerning between neutral and charged polyene chains, whose position in wavenumber is almost unaffected by the chain lengths.

The strong Raman band observed at 253 cm^{-1} (ν_{24}) corresponds to a deformation delocalized over the whole molecule. This mode is regarded as one of the longitudinal acoustic modes (LAMs). As shown in Table 8, vibrations along five coordinates contribute significantly to the Raman intensity of this mode. Other LAMs appear as weak Raman bands at 615 and 475 cm^{-1} (ν_{21} and ν_{22}).

The calculated skeletal stretching force constants [scaled by $(0.933)^2$] are shown in Table 9. While the diagonal force constants for the N−methyl stretches [4.821 mdyn Å^{-1} for $\sigma(N_LC_\alpha)$ and 4.860 mdyn Å^{-1} for $\sigma(N_LC_\beta)$] are typical for N−C stretches, the diagonal force constant of 8.376 mdyn Å^{-1} calculated for $\sigma(N_LC_1)$ is in the middle of typical values for the N−C and N═C bonds. The diagonal force constants for $\sigma(C_1C_2)$ and $\sigma(C_2C_3)$ (6.712 and 6.692 mdyn Å^{-1}, respectively) are very close to each other and are in the middle of typical values for the C−C and C═C bonds, corresponding to the result shown in section 3A that there is virtually no bond alternation in the conjugated chain of SC5OP.

The off-diagonal force constants for the NC and CC bond stretches in the conjugated chain are large in magnitude and decrease slowly as the relevant bonds become distant. For example, the coupling constants between adjacent CC bonds are as large as 0.6−0.7 mdyn Å^{-1}, which is larger than those calculated for *all-trans*-decapentaene (0.4−0.5 mdyn Å^{-1}, after scaling at the MP2/6-31G* level).[13] The coupling constant between $\sigma(C_1C_2)$ and $\sigma(C_4C_5)$, although separated by two CC bonds, is 0.181 mdyn Å^{-1}, which is more than twice as large as the corresponding value in *all-trans*-decapentaene (0.06−0.08 mdyn Å^{-1}). This result indicates that the conjugated chain of SC5 is a system correlated more strongly than neutral polyene chains and is related to the strong electron−vibration interaction giving rise to a large charge flux for the bond-alternation coordinate discussed above, as well as to the strong dependence of the IR spectrum in the 1700−1450-cm^{-1} region on theoretical levels discussed in section 3C.

4. Concluding Remarks

It has been shown in the present study that the observed features of the IR and Raman spectra of SC5 are well reproduced by the calculations for SC5OP at the BHandHLYP/6-31G* level. Detailed examination of the origin of the IR and Raman intensities and the vibrational force constants derived from the calculations has shown that the conjugated chain of SC5OP is a system correlated more strongly than neutral polyene chains. It is hoped that such knowledge of electron−vibration interactions in SC5 would be useful for understanding and controlling the electronic properties of cyanine dyes in general, which are known to have various practical applications.

Acknowledgment. The authors thank Dr. Y. Watanabe for performing the calculation at the MP2/6-31G* level on a CRAY Y-MP supercomputer.

References and Notes

(1) West, W.; Gilman, P. B., Jr. In *The Theory of the Photographic Process*, 4th ed.; James, T. H., Ed.; Macmillan: New York, 1977; Chapter 10.
(2) Herz, A. H. In *The Theory of the Photographic Process*, 4th ed.; James, T. H., Ed.; Macmillan: New York, 1977; Chapter 9.
(3) Herz, A.; Danner, R.; Janusonis, G. *Adsorption from Aqueous Solution*; Advances in Chemistry Series 79; American Chemical Society: Washington, DC, 1968; p 173.
(4) McRae, E. G.; Kasha, M. *J. Chem. Phys.* **1958**, *28*, 721.
(5) Scheibe, G.; Haimerl, F.; Hoppe, W. *Tetrahedron Lett.* **1970**, 3067.
(6) Maskasky, J. E. *Langmuir* **1991**, *7*, 407.
(7) Saito, H.; Isshiki, T.; Shiojiri, M.; Ohtani, H.; Ning, G.; Ogawa, K. *J. Imag. Sci. Technol.* **1993**, *37*, 348.
(8) Sano, N.; Shimizu, M.; Tanaka, J.; Tasumi, M. *J. Raman Spectrosc.* **1988**, *19*, 395.
(9) Brandt, E. S. *Appl. Spectrosc.* **1988**, *42*, 882.
(10) He, T.-J.; Lin, C.-S.; Xin, H.-W.; Liu, F.-C. *J. Photogr. Sci.* **1989**, *37*, 2.
(11) Wang, J.; Zhang, P.; He, T.; Xin, H.; Liu, F.-C. *J. Phys. Chem.* **1988**, *92*, 1942.
(12) Iwata, K.; Weaver, W. L.; Gustafson, T. L. *J. Phys. Chem.* **1992**, *96*, 10219.
(13) Hirata, S.; Yoshida, H.; Torii, H.; Tasumi, M. *J. Chem. Phys.* **1995**, *103*, 8955.
(14) Hirata, S.; Torii, H.; Tasumi, M. *J. Chem. Phys.* **1995**, *103*, 8964.
(15) Kofranek, M.; Lischka, H.; Karpfen, A. *J. Chem. Phys.* **1992**, *96*, 982.
(16) Torii, H.; Tasumi, M. *J. Phys. Chem. B* **1997**, *101*, 466.
(17) Frisch, M. J.; Trucks, G. W.; Schlegel, H. B.; Gill, P. M. W.; Johnson, B. G.; Wong, M. W.; Foresman, J. B.; Robb, M. A.; Head-Gordon, M.; Replogle, E. S.; Gomperts, R.; Andres, J. L.; Raghavachari, K.; Binkley, J. S.; Gonzalez, C.; Martin, R. L.; Fox, D. J.; Defrees, D. J.; Baker, J.; Stewart, J. J. P.; Pople, J. A. *Gaussian 92/DFT*; Gaussian, Inc.: Pittsburgh, PA, 1993.
(18) Frisch, M. J.; Trucks, G. W.; Schlegel, H. B.; Gill, P. M. W.; Johnson, B. G.; Robb, M. A.; Cheeseman, J. R.; Keith, T.; Petersson, G. A.; Montgomery, J. A.; Raghavachari, K.; Al-Laham, M. A.; Zakrzewski, V. G.; Ortiz, J. V.; Foresman, J. B.; Cioslowski, J.; Stefanov, B. B.; Nanayakkara, A.; Challacombe, M.; Peng, C. Y.; Ayala, P. Y.; Chen, W.; Wong, M. W.; Andres, J. L.; Replogle, E. S.; Gomperts, R.; Martin, R. L.; Fox, D. J.; Binkley, J. S.; Defrees, D. J.; Baker, J.; Stewart, J. J. P.; Head-Gordon, M.; Gonzalez, C.; Pople, J. A. *Gaussian 94*; Gaussian, Inc.: Pittsburgh, PA, 1995.
(19) Becke, A. D. *Phys. Rev. A* **1988**, *38*, 3098.
(20) Lee, C.; Yang, W.; Parr, R. G. *Phys. Rev. B* **1988**, *37*, 785.
(21) Miehlich, B.; Savin, A.; Stoll, H.; Preuss, H. *Chem. Phys. Lett.* **1989**, *157*, 200.
(22) Becke, A. D. *J. Chem. Phys.* **1993**, *98*, 5648.
(23) Becke, A. D. *J. Chem. Phys.* **1993**, *98*, 1372.
(24) Komornicki, A.; McIver, J. W., Jr. *J. Chem. Phys.* **1979**, *70*, 2014.
(25) Honda, M.; Katayama, C.; Tanaka, J. *Acta Crystallogr. B* **1986**, *42*, 90.
(26) Yannoni, C. S.; Clarke, T. C. *Phys. Rev. Lett.* **1983**, *51*, 1191.
(27) Gussoni, M.; Castiglioni, C.; Zerbi, G. In *Spectroscopy of Advanced Materials*; Clark, R. J. H., Hester, R. E. Eds.; Advances in Spectroscopy 19; Wiley: New York, 1991; p 251.
(28) Zerbi, G.; Castiglioni, C.; Sala, S.; Gussoni, M. *Synth. Met.* **1987**, *17*, 293.
(29) Szalay, P. G.; Karpfen, A.; Lischka, H. *J. Chem. Phys.* **1987**, *87*, 3530.
(30) Guo, H.; Karplus, M. *J. Chem. Phys.* **1991**, *94*, 3679.
(31) Champagne, B.; Perpète, E. A.; André, J.-M. *J. Chem. Phys.* **1994**, *101*, 10796.
(32) Torii, H.; Tasumi, M. *J. Chem. Phys.* **1994**, *101*, 4496.

(33) Goodman, L.; Ozkabak, A. G.; Thakur, S. N. *J. Phys. Chem.* **1991**, *95*, 9044.
(34) Brenner, L. J.; Senekowitsch, J.; Wyatt, R. E. *Chem. Phys. Lett.* **1993**, *215*, 63.
(35) Handy, N. C.; Murray, C. W.; Amos, R. D. *J. Phys. Chem.* **1993**, *97*, 4392.
(36) Torii, H.; Tasumi, M. *J. Mol. Struct. (THEOCHEM)* **1995**, *334*, 15.
(37) Torii, H.; Tasumi, M. *J. Mol. Struct.* **1996**, *376*, 317.
(38) Torii, H.; Tasumi, M.; Bell, I. M.; Clark, R. J. H. *Chem. Phys.* **1997**, *216*, 67.
(39) Horovitz, B. *Solid State Commun.* **1982**, *41*, 729.
(40) Masuda, S.; Torii, H.; Tasumi, M. *J. Phys. Chem.* **1996**, *100*, 15335.
(41) Torii, H.; Furuya, K.; Tasumi, M. *J. Phys. Chem. A* **1998**, *102*, 8422.
(42) Harada, I.; Furukawa, Y.; Tasumi, M.; Shirakawa, H.; Ikeda, S. *J. Chem. Phys.* **1980**, *73*, 4746.
(43) Uchida, Y.; Furukawa, Y.; Tasumi, M. *Synth. Met.* **1995**, *69*, 55.